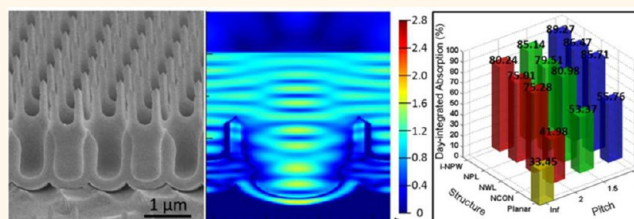


Efficient Light Absorption with Integrated Nanopillar/Nanowell Arrays for Three-Dimensional Thin-Film Photovoltaic Applications

Qingfeng Lin, Bo Hua, Siu-fung Leung, Xicheng Duan, and Zhiyong Fan*

Department of Electronic and Computer Engineering, Hong Kong University of Science and Technology, Clear Water Bay, Kowloon, Hong Kong, China SAR

ABSTRACT Efficient light absorption in thin-film photovoltaic (PV) devices is crucial for improving their efficiency and reducing cost. Here we have not only developed a low-cost and scalable method to fabricate a unique type of integrated-nanopillar-nanowell (i-NPW) structure by integrating nanopillar and nanowell arrays together vertically, but also demonstrated the attractive optical property of the i-NPW arrays by leveraging the advantages of “positive” and “negative” nanostructures for photon harvesting. Impressively, the 2 μm thick i-NPW arrays with only 40 nm a-Si coating obtained a day-integrated absorption of 89.27%, as opposed to only 33.45% for the planar control sample. These results suggest the feasibility and clear advantage of vertical integration of three-dimensional (3-D) nanophotonic structures, and meanwhile also pave a viable and convenient way toward a 3-D ultrathin film PV module with potency for high energy conversion efficiency.



KEYWORDS: efficient light absorption · thin-film photovoltaics · three-dimensional nanophotonic structures · vertically integrated-nanopillar-nanowell structures · day-integrated absorption

Efficient light absorption is crucial for enhancing the performance of thin-film photovoltaic (PV) devices, which requires both broadband antireflection coatings and efficient light trapping techniques. Properly engineered three-dimensional (3-D) photonic nanostructures have demonstrated highly promising capability of harvesting sunlight over a broad range of wavelengths and incident angles.^{1–6} In particular, arrays of a variety of 3-D nanostructures, such as nanowires,^{7–10} nanopillars (NPLs),^{11,12} nanowells (NWLs),^{1,13,14} nanocones,^{3,4,15} nanopyramids,^{16–18} nanospheres,^{19–21} and so forth, have been extensively studied for light trapping and solar energy conversion with photonic materials including Si,^{3,7,8,18} Ge,^{5,11} CdS,¹² and Cu(In, Ga)Se (CIGS),⁶ etc. By rational integration of these 3-D nanostructures, photons can be trapped efficiently within the thin-film absorber layer, consequently improving light absorption and thus conversion efficiencies. Additionally, enhanced absorption efficiency leads to utilization of a thinner absorber layer, which

improves carrier collection, as well as reduces production costs and environmental concern for solar cells made of rare materials, for example, CIGS, and environmentally unfriendly material, for example, CdTe. Our previous work demonstrated that a properly designed 3-D NWL array fabricated by a low-cost and scalable approach can serve as an efficient photon harvester confirmed by both experiments and simulations systematically.¹ In this work, it was found that highly regular NPL arrays can be fabricated with precisely controlled wet chemical etching after obtaining 3-D NWL arrays. In addition, a unique integrated-NPL-NWL (i-NPW) structure has been successfully realized by carefully designing and controlling the wet etching and anodization processes. Furthermore, systematic optical property investigations on the obtained 3-D structures have been performed experimentally, assisted with optical simulations. It was found that NWL arrays with cylindrical cavities provide efficient geometric confinement for normal incident incoming photons naturally, while

* Address correspondence to eezfan@ust.hk.

Received for review January 11, 2013 and accepted February 11, 2013.

Published online February 12, 2013
10.1021/nn400160n

© 2013 American Chemical Society

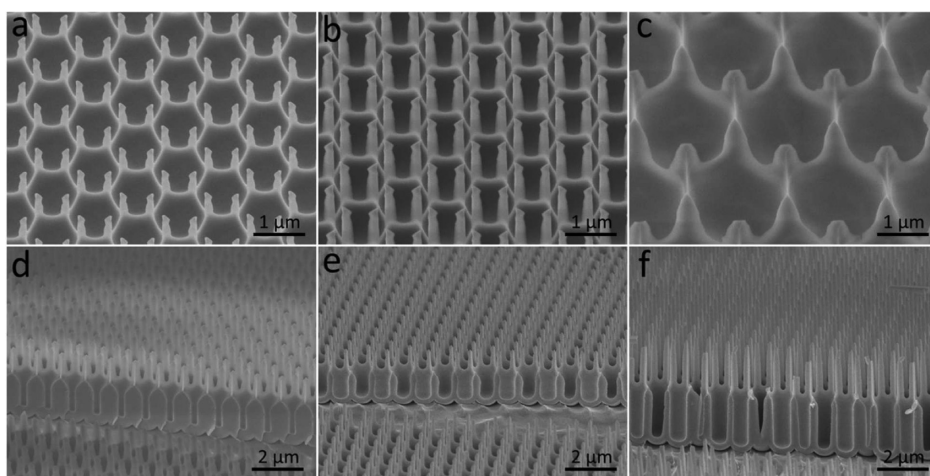


Figure 1. SEM images at 60° tilted-angle-view of NPL structures with (a) 1 μm pitch and 1 μm height, (b) 1 μm pitch and 2 μm height, and (c) 2 μm pitch and 2 μm height. Cross-sectional view SEM images of 1 μm pitch i-NPW structures made by (d) 1 μm height NPLs on 1 μm depth NWLs with 285 nm well diameter, (e) 1 μm height NPLs on 1 μm depth NWLs with 710 nm well diameter, (f) 2 μm height NPLs on 2 μm depth NWLs with 710 nm well diameter.

NPL arrays with small diameter tips lead to a broadband suppression of reflectance with superior angular absorption performance. Therefore, a rational vertical integration of the two types of 3-D nanostructures, that is, i-NPW, leads to a much improved photon harvesting property over a large wavelength and incident angle range. These results not only shed light on the light trapping mechanism in complex 3-D nanophotonic structures but also provide a facile approach to fabricate the 3-D nanostructures for ultrathin film photovoltaics.

RESULTS AND DISCUSSION

The unique NPL arrays in this work were fabricated by nanoimprint-assisted anodization of aluminum (Al) foil in conjunction with precise wet chemical etching. The detailed fabrication procedure of hexagonally ordered NPLs is schematically shown in Supporting Information Figure S1. Conventionally, Al anodization is used to form self-organized nanoporous alumina structures,²² which have been widely utilized as nanoengineering templates for direct assembly of nanomaterials.^{11,12,23–25} However, there was no report on fabrication of regular NPL arrays with periodicity comparable to that of a visible optical wavelength owing to the challenge of stable anodization of Al with high voltage.^{26,27} In this work, our recently developed high voltage Al anodization process was adopted; thus the large pitch NWL arrays were achieved.¹ Thereafter, wet chemical etching was performed to partially etch away alumina, and highly regular NPL arrays were formed by precisely controlling the etching time. Figure 1 panels a–c demonstrate 60° tilted-angle-view scanning electron microscopy (SEM) images of NPL structures with tunable pitches and heights. Particularly, 1 μm pitch NPLs with a height of 1 μm , 1 μm pitch NPLs with a height of 2 μm , and 2 μm pitch NPLs with a height of 2 μm are shown respectively. Note that in this work,

free-standing NPL arrays have been well obtained *via* precise control of wet chemical etching without any special surface treatment, ascribed to their relatively small aspect ratio and the precisely controlled large pitch. It is worth pointing out that the NPLs fabricated here have a tapered structure as shown in Figure 1a–c, which are different from conventional NPLs with uniform diameters. The tapered structure provides a gradual change of effective refractive index of the entire 3-D structure, leading to greatly reduced reflectance for the incoming photon,²⁸ similar to the case of nano-needles, nanocones, and nanospikes.^{2–6,29} Such NPL arrays can serve as templates for 3-D thin-film photovoltaics which have been demonstrated before.^{6,29–32} The significant advantages of the approach developed here rest in the fact that the cost of substrate material and fabrication process is much lower than that of the conventional lithographic methods for fabrication of 3-D NPL and NWL arrays.^{7,8,14} In addition, an Al foil is also much lighter and more flexible than the conventional Si and glass substrates, which is attractive for practical applications.

To implement precise control of the wet etching process for fabrication of NPLs, an *in-situ* optical reflectance monitoring system was setup to measure the reflectance change of the 3-D structure on an Al substrate, as schematically shown in Supporting Information, Figure S2a. In brief, a diode laser with wavelength 650 nm was focused onto the 3-D structure with a small incident angle, and a Si photodetector was used to detect the intensity of the zero-order diffraction beam. Because of the structural transition from NWLs to NPLs (insets of Supporting Information, Figure S2b), the structural effective refractive index changes over time during the etching process, leading to the observable reflectance oscillation shown in Figure S2b. Empirically, the etching time in order to form NPLs was

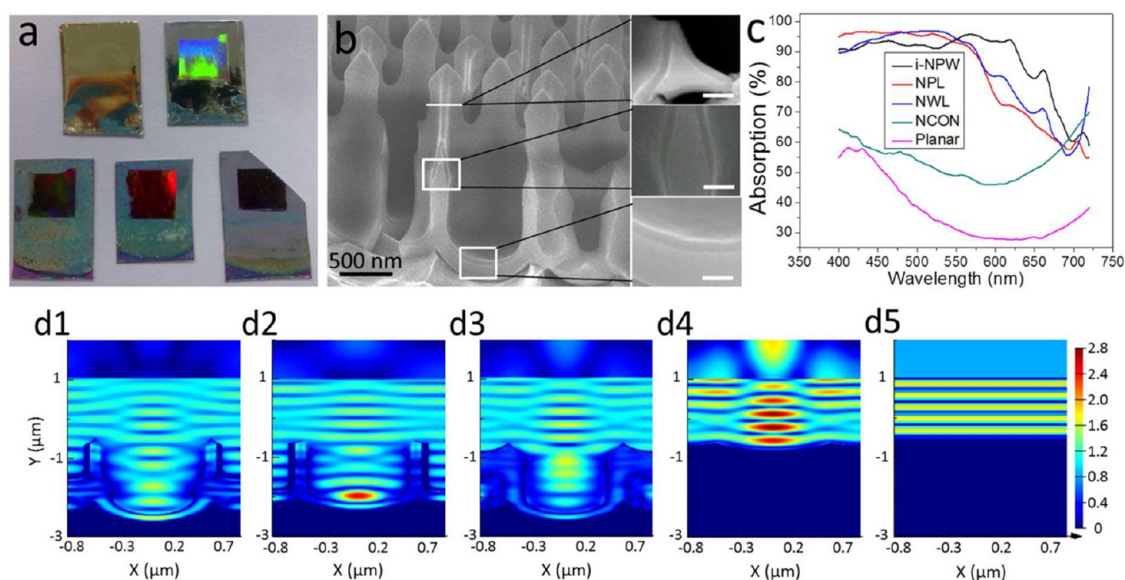


Figure 2. (a) Photograph of five samples with planar, NCONs, NWLs, NPLs, and i-NPWs structures after 40 nm a-Si conformal coating (from top to bottom, left to right). (b) Cross-sectional SEM image of 1 μm pitch i-NPW arrays with 40 nm a-Si coating (right), and higher magnified SEM images of particular parts of the i-NPW structure (left, the scale bars here are 100 nm). (c) The normal incident absorption spectra of the five samples in panel a. (d1–d5) Simulated cross-sectional $|E|^2$ distribution of the EM wave on i-NPWs, NPLs, NWLs, NCONs, and planar, respectively.

identified and it was found that more etching beyond 100 min results in complete removal of alumina and planarization of the supporting Al substrate, thus greatly enhancing specular reflectance, as is evident in Figure S2b.

It can be seen that formation of NWLs and NPLs depends on control of the wet etching condition, therefore, a vertically integrated complex structure, that is, i-NPW, can be fabricated following the process flow shown in Supporting Information, Figure S3. This unique i-NPW structure provides the possibility for more efficient light absorption by combining the advantages of “positive” and “negative” structures.¹ Figure 1d–f demonstrate cross-sectional view SEM images of 1 μm pitch i-NPW structures with tunable height and NWL sizes, particularly, 1 μm height NPLs integrated on 1 μm depth NWLs with 285 nm well diameter, 1 μm height NPLs on 1 μm depth NWLs with 710 nm well diameter, 2 μm height NPLs on 2 μm depth NWLs with 710 nm well diameter are shown, respectively. All the SEM images in Figure 1 present evidence of the controllability of the NPL and i-NPW arrays fabricated here.

As mentioned previously, arrays of a variety of 3-D nanostructures have demonstrated highly promising capability of harvesting sunlight over a broad range of wavelengths and incident angle. To investigate the light trapping property of the unique i-NPW arrays, 40 nm a-Si thin-films were deposited on the structures serving as light absorbers *via* the plasma-enhanced chemical vapor deposition (PECVD) method. For comparison, the same thickness of a-Si thin-films were also deposited on NPLs, NWLs, nanoconcaves (NCONs,

Supporting Information Figure S1d), and electropolished flat Al substrate. Figure 2a shows a photograph of five samples after 40 nm a-Si conformal coating (from top to bottom, left to right) with planar, NCONs, NWLs, NPLs, and i-NPWs structures, respectively. Note that the later four nanostructures have the same pitch of 1 μm , the last three ones have a thickness/height of 2 μm , and i-NPWs have a 1 μm thick NPLs layer and 1 μm thick NWLs layer. To acquire the optimal broadband absorption, both NWLs and i-NPWs have a well diameter of 870 nm.¹ Figure 2b shows cross-sectional SEM image of 1 μm pitch i-NPW arrays with 40 nm a-Si coating (left), and higher magnified images of particular parts of the i-NPW structure (right), illustrating the conformal a-Si coating over the 3-D structures. To quantitatively characterize optical properties of these structures, UV–vis reflectance spectra were obtained with an integrating sphere. Their absorption spectra were obtained by subtracting reflectance from unity as the samples are opaque. Figure 2c demonstrates the normal incident absorption spectra of the five structures in Figure 2a. It is known that a-Si has an optical band gap of ~ 1.7 eV, corresponding to ~ 720 nm optical wavelength. Therefore, spectral range 400–720 nm was chosen to investigate above-band gap optical absorption of these structures. On the other hand, this wavelength range has covered the peak of solar irradiance, thus the results are meaningful for further thin-film PV applications. Note that the lower boundary of the wavelength range is limited by the home-built measurement setup. As it can be clearly observed in Figure 2c, i-NPWs have a higher broadband absorption than NPLs and NWLs, especially for long wavelengths. NCONs' broadband

absorption is much poorer than the former three types of 3-D nanostructures. And planar structure has the worst absorption capability. To verify the experimental results, as well as to understand how light is trapped in these structures, finite-difference-time-domain (FDTD) simulations were performed on these structures at 600 nm wavelength, and the cross-sectional electric field intensity ($|E|^2$) distribution of the electromagnetic (EM) wave was plotted as shown in Figure 2d. In these five simulations, EM plane waves propagate downward from $Y = 1 \mu\text{m}$ and reach the top surfaces of these structures at about $Y = -0.5 \mu\text{m}$. Note that the color index at the specific location in the simulations reflects the magnitude of $|E|^2$ at that point, normalized with that of the source EM wave if propagating in free space. It can be observed that i-NPWs demonstrate quite low reflectance, indicated by the weak interference fringes (Figure 2d1). On the other hand, NPLs and NWLs show slightly higher reflectance due to inefficient photon absorption of the trapped light (Figure 2d2), and reflection by large top structure surface area (Figure 2d3), respectively. Nevertheless, all the above three types of nanostructures perform much better than the NCONs and planar substrate, which demonstrate much stronger reflectance from their top surfaces (Figure 2d4, 2d5). Low reflectance of the i-NPW arrays indicates an efficient light absorption in the structures, which is attributed to a combinational effect of reduced broadband reflection due to tapered tips on the top, and efficient light trapping of the penetrating photons in the cylindrical cavities at the bottom.

The results shown above suggest that PV material coated i-NPW arrays are excellent photon harvesting structures. In fact, although there have been many reports on a variety of 3-D “positive” and “negative” nanostructures for efficient light trapping, the unique i-NPW structure combines both “positive” and “negative” nanostructures, possessing NPLs on the top for minimal reflectance and NWLs on the bottom for efficient light capturing, leading to an impressively efficient light absorption. Therefore, as compared to planar thin-film PV devices, much thinner light absorber layers are required for sufficient light absorption on i-NPW structures. A thinner light absorber is beneficial for many nano/microcrystalline thin-film PV devices owing to the shortened minority carrier migration path and improved carrier collection efficiency.^{8,12,31} Especially for a-Si PV devices, the Staebler-Wronski effect associated performance degradation can be mitigated by using thinner a-Si layer.^{33,34} In addition, as the thickness/height of the i-NPW arrays is only $2 \mu\text{m}$, they can be readily detached from Al substrate and embedded in flexible substrate,^{1,12} which is highly attractive for flexible PV applications.

Notably, the above optical measurements were performed with normal incident light, while for practical PV applications, light absorption from angular incident has to be considered because of the change

of solar irradiation angle over the time during the day time. Accordingly, we have investigated the angular absorption property of NWL, NPL, and i-NPW arrays with $1 \mu\text{m}$ pitch and 40 nm a-Si coating with an integrating sphere. Particularly, the light incident angle was tuned from 0° to 60° with 10° interval, and a full spectral reflectance curve was obtained for each angle. As mentioned above, absorption spectra were then calculated by subtracting reflectance from unity since there was no transmission. It can be observed from Figure 3a,b, that NWL arrays have a slightly better broadband absorption for small angle incident than NPL arrays especially for long wavelength, while the later ones perform much better for large angle incident. This is because for small angle incident, NWL arrays can confine the incoming photon more efficiently with their cylindrical cavities; while for large angle incident, NPL arrays have a suppressed reflection because of their tapered tops leading to much smaller effective refractive index and more photon travel path length at large incident angle. By combining the advantages of these two nanostructures, i-NPW arrays have the capability to achieve the best broadband absorption over the whole range of incident angles (Figure 3c). To evaluate the incident angle-dependent broadband absorption capability of these 3-D nanostructures more clearly, their absorption spectra were integrated with the solar photon flux spectrum (AM1.5G)³⁵ in the range of 400–720 nm (Supporting Information), resulting in above-band gap broadband photon flux absorption shown in Figure 3d. The AM1.5G photon flux absorption clearly indicates that NWLs demonstrate a better broadband absorption than NPLs when the incident angle is small, while NPLs possess a much better AM1.5G photon flux absorption when the incident angle is large. This intriguing effect can be explained as follows. An NWL structure has higher material filling ratio than an NPL structure in addition to efficient cavity light trapping, resulting in better absorption for normal incident photons. However, it also has a larger top surface area than an NPL structure, therefore when the incident light tilts away from normal gradually, although in the beginning the photon travel path in both structures increases leading to improved absorption in both cases, further tilting results in more increased top surface reflectance for the NWL structure than the NPL structure, thus leading to a faster decay of absorption when the angle is larger than 30° in Figure 3d. By integrating NPLs and NWLs together vertically, i-NPWs demonstrate the best broadband absorption over all incident angles with small dependence on incident angle, combining the advantages of NWLs and NPLs. Additionally, we also obtained the angular dependent absorption spectra for $1 \mu\text{m}$ pitch NCONs and planar (Supporting Information Figure S4), which are much worse than the above three types of 3-D nanostructures.

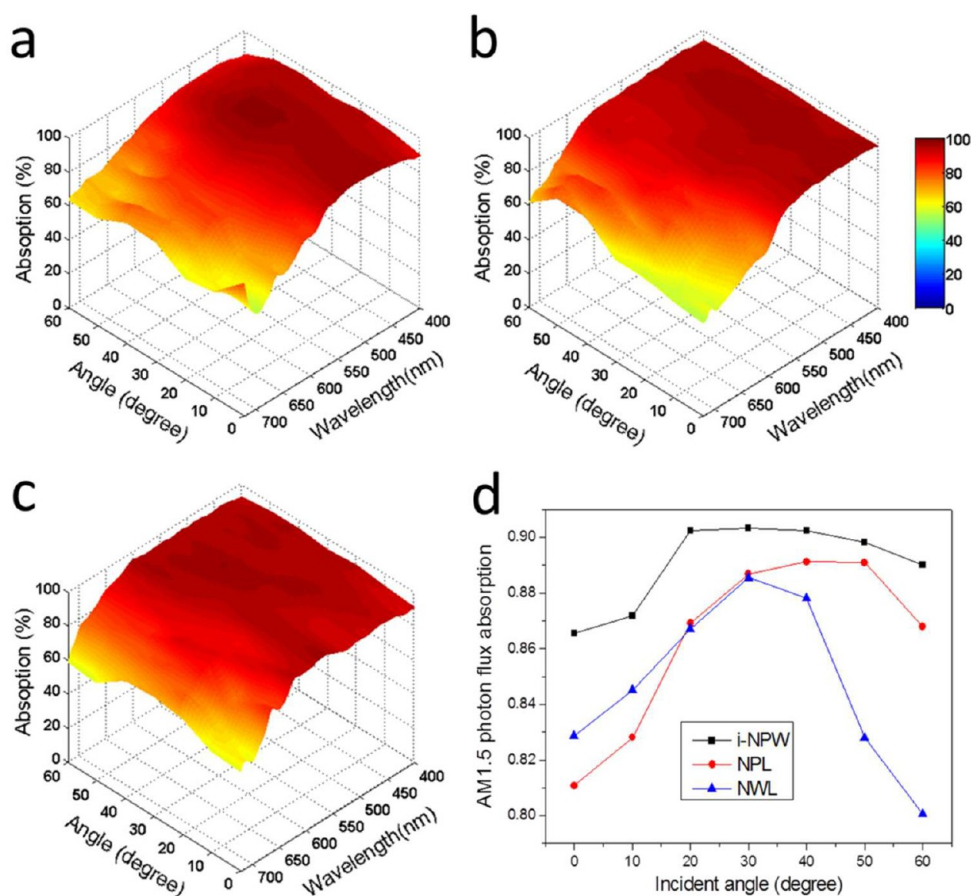


Figure 3. Angular- and wavelength-dependent absorption spectra of (a) NWLs, (b) NPLs, and (c) i-NPWs with 1 μm pitch and 40 nm a-Si coating. (d) Above-band gap broadband photon flux absorption with incident angle dependence of NWLs, NPLs, and i-NPWs.

To investigate the effect of the pitch of the nanostructures on their light trapping property, NCONs, NWLs, NPLs, and i-NPWs with 1.5 and 2 μm pitches were also fabricated. Like their 1 μm pitch counterparts, all the later three types of 3-D nanostructures have a height of 2 μm ; NWLs and i-NPWs have the optimal well diameter for maximum absorption efficiency of 1360 nm for 1.5 μm pitch, and 1700 nm for 2 μm pitch, respectively. The angular dependent absorption spectra for these nanostructures with 40 nm a-Si coating were also performed, as shown in Supporting Information Figures S5 and S6. By comparing Figure 3 and Figures S5 and S6, it can be observed that for the same type of nanostructures, the 1 μm pitch nanostructure has a better absorption over all incident angles than its 1.5 μm pitch counterpart followed by 2 μm pitch nanostructures. These results are consistent with our previous observation on NWL arrays.¹ In addition, for the samples with the same pitch, there is a similar relationship about absorption efficiency between different types of nanostructures as observed above. Note that although our previous work on NWL arrays revealed that 700 nm pitch NWL arrays with large pore size show the best absorption efficiency than its larger pitches, the overall thickness of contact

electrode layer and active absorber layer for practical thin-film PV devices is normally a few hundred nanometers,^{30,32} thus they cannot be deposited uniformly onto 700 nm pitch 3-D nanostructures. Therefore choosing pitch of 1 μm and above for investigation has practical meaning.

Following the angular dependent absorption measurements above, the angular absorption spectra of all the structures were integrated with AM1.5G solar photon flux spectrum (Supporting Information), as illustrated in Figure 4a, showing above-band gap broadband absorption for all the structures *versus* incident angle. Figure 4a summarizes quantitatively the results observed above. First, NCONs have a broadband absorption better than that of planar over all incident angles, while NWLs, NPL, and i-NPWs have a broadband absorption much better than that of NCONs and planar. Second, for a particular type of nanostructures, the one with 1 μm pitch shows higher broadband absorption over all incident angles than the one with 1.5 μm pitch, which is then better than the one with 2 μm pitch. Third, for the different types of nanostructures with the same pitch, i-NPWs outperform NWLs and NPLs over all incident angles. Note that the ideal photocurrent density was also shown in

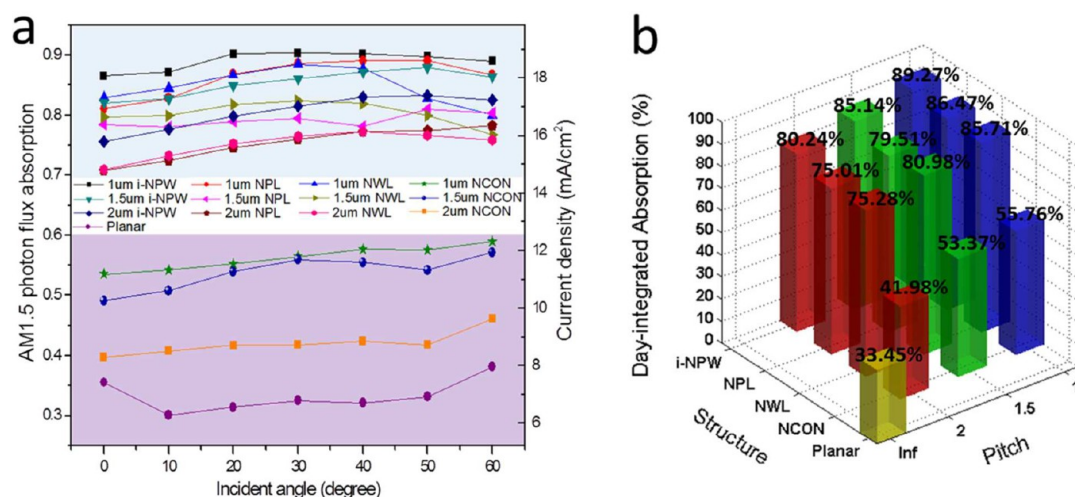


Figure 4. (a) Above-band gap broadband photon flux absorption with incident angle dependence of all the structures, with their photocurrent density showing in the right y axis based on the assumption that there is no recombination loss. (b) Day-integrated solar energy absorption of all the structures.

Figure 4a to give a reference of the expected PV device performance, based on the assumption that there is no recombination loss (Supporting Information). As discussed above, angular absorption of 3-D nanostructures needs to be explored for practical PV applications. Therefore, day-integrated solar energy absorption was calculated and shown in Figure 4b following the approach developed by us previously.² It can be seen that 1 μm pitch i-NPW arrays show 89.27% absorption over the 8 h period of one day, while there is only 33.45% absorption for the planar control sample. And for a particular pitch, NWLs and NPLs have similar day-integrated absorption, lower than that of i-NPWs but much higher than that of NCONs.

CONCLUSION

Although a variety of 3-D nanostructures have been widely studied for efficient light trapping, there have very few reports on rational integration of different types of nanostructures to leverage their advantages

for photon harvesting. In this work, we have not only demonstrated a low-cost and scalable method to fabricate a unique type of i-NPW structure, by integrating NPL and NWL arrays together vertically, but also demonstrated the attractive optical property of the i-NPW arrays experimentally assisted with optical simulations. It was discovered that the integrated nanostructures combining both “positive” and “negative” nanostructures show more efficient light absorption than the “positive” or “negative” nanostructures alone over a broad range of wavelengths and incident angles. Impressively, the 2 μm thick i-NPW arrays with only 40 nm a-Si coating obtained a day-integrated absorption of 89.27%, as opposed to only 33.45% for the planar control sample. These results suggest the feasibility and clear advantage of vertical integration of 3-D nanophotonic structures, and meanwhile also pave a viable and convenient way toward 3-D ultrathin film PV module with potency for high energy conversion efficiency.

METHODS

NPL Arrays Fabrication. Fabrication procedure of hexagonally ordered NPLs is schematically shown in Supporting Information, Figure S1. In detail, aluminum (Al) foil with a thickness of 0.25 mm (99.99% Alfa Aesar) was cut into small pieces and cleaned in acetone and isopropyl alcohol. The substrates were electrochemically polished in a 1:3 (v/v) mixture of perchloric acid and ethanol for 4 min at 5 $^{\circ}\text{C}$. After polishing, the substrates were imprinted by silicon mold (hexagonally patterned pillar with height of 200 nm, diameter of 200–500 nm and pitches ranging from 1 to 2 μm) with a pressure of $\sim 1.1 \times 10^4 \text{ N cm}^{-2}$ to initiate the perfectly ordered NPL growth as shown in Supporting Information, Figure S1a,b. The substrates were first anodized with proper conditions to form an ordered alumina channels layer, which was then etched away in a mixture of phosphoric acid (6 wt %) and chromic acid (1.8 wt %) at 63 $^{\circ}\text{C}$ for 50 min (Supporting Information, Figure S1d). Afterward, the substrates were second anodized under the same condition as first anodization to obtain 2 μm thick NWL arrays

(Supporting Information, Figure S1e). In the end, NPL arrays were obtained *via* precisely controlled wet etching with 5 wt % phosphoric acid at 53 $^{\circ}\text{C}$ (Supporting Information, Figure S1f).

In-Situ Optical Reflectance Monitoring. The *in-situ* optical reflectance monitoring system for implementing precise control of the wet etching process for fabrication of NPLs is schematically shown in Supporting Information, Figure S2a. Here we studied the real-time change of effective refractive index of three identical 1 μm pitch samples with 2 μm alumina thickness. Note that when 650 nm light was focused onto 1 μm pitch alumina structure, there were one zero-order diffraction beam and 6 first-order diffraction beams according to the diffraction grating theory.³⁶ The intensity of the zero-order diffraction beam was measured yielding reflectance with arbitrary unit (au). Supporting Information, Figure S2b demonstrates three reflectance curves with peaks and valleys located at almost the same etching time, which indicates the change of effective refractive index of the entire structure with the proceeding of wet

chemical etching. The NPL arrays were formed at 80 min etching time.

i-NPW Arrays Fabrication. Fabrication process of vertically integrated i-NPW arrays is schematically shown in Supporting Information, Figure S3, starting from second anodization. To achieve i-NPW arrays, the substrates were second anodized for time t_{A1} using the same anodization conditions (Supporting Information, Figure S3a) and etched in 5 wt % phosphoric acid at 53 °C for t_{E1} (Supporting Information, Figure S3b). Then the third anodization step at the same conditions was performed for another time t_{A2} (Supporting Information, Figure S3c) followed by phosphoric acid etch for time t_{E2} to obtain NPLs on the top (Supporting Information, Figure S3d). Note that in this scenario the NPLs segment was etched for $t_{E1} + t_{E2}$, while the NWLs segment was etched for t_{E2} .

Microscopy and Spectroscopy. SEM images of the 3-D nanostructures were obtained using a JEOL JSM-6700F SEM working at 5 kV. Angular- and wavelength-dependent absorption spectra of all structures were carried out on a home-built UV–vis measurement system, made by a spectrometer equipped with an integrating sphere.

Conflict of Interest: The authors declare no competing financial interest.

Acknowledgment. The authors thank Mr. Kwong-Lung Ching and Qianpeng Zhang for technical assistance. This work was partially supported by General Research Fund (612111) from Hong Kong Research Grant Council, HKUST Research Project Competition Grant (RPC11EG38), National Research Foundation of Korea funded by the Korean Government (NRF-2010-220-D00060, 2008-0662256), HKUST Special Research Fund Initiative (SRF11EG17), and Hong Kong Innovation and Technology Fund (ITS/192/11) from the Innovation and Technology Commission.

Supporting Information Available: Schematics of NPLs fabrication are illustrated in Figure S1, schematic of the *in-situ* optical reflectance monitoring system, and reflectance curves of 3 identical 1 μ m pitch samples with 2 μ m alumina thickness during the wet etching process are demonstrated in Figure S2, schematics of i-NPWs fabrication are illustrated in Figure S3, angular- and wavelength-dependent absorption spectra of 40 nm a-Si layer on 1 μ m pitch NCONs and planar are shown in Figure S4, angular- and wavelength-dependent absorption spectra of NWLs, NPLs, i-NPWs, and NCONs with 1.5 μ m pitch and 40 nm a-Si coating are shown in Figure S5, angular- and wavelength-dependent absorption spectra of NWLs, NPLs, i-NPWs, and NCONs with 2 μ m pitch and 40 nm a-Si coating are shown in Figure S6. This material is available free of charge via the Internet at <http://pubs.acs.org>.

REFERENCES AND NOTES

- Leung, S. F.; Yu, M.; Lin, Q.; Kwon, K.; Ching, K. L.; Gu, L.; Yu, K.; Fan, Z. Efficient Photon Capturing with Ordered Three-Dimensional Nanowell Arrays. *Nano Lett.* **2012**, *12*, 3682–3689.
- Yu, R.; Ching, K.; Lin, Q.; Leung, S.; Arcrossito, D.; Fan, Z. Strong Light Absorption of Self-Organized 3-D Nanospire Arrays for Photovoltaic Applications. *ACS Nano* **2011**, *5*, 9291–9298.
- Zhu, J.; Yu, Z. F.; Burkhard, G. F.; Hsu, C. M.; Connor, S. T.; Xu, Y. Q.; Wang, Q.; McGehee, M.; Fan, S. H.; Cui, Y. Optical Absorption Enhancement in Amorphous Silicon Nanowire and Nanocone Arrays. *Nano Lett.* **2009**, *9*, 279–282.
- Wang, K. X.; Yu, Z.; Liu, V.; Cui, Y.; Fan, S. Absorption Enhancement in Ultrathin Crystalline Silicon Solar Cells with Antireflection and Light-Trapping Nanocone Gratings. *Nano Lett.* **2012**, *12*, 1616–1619.
- Chueh, Y. L.; Fan, Z. Y.; Takei, K.; Ko, H.; Kapadia, R.; Rathore, A.; Miller, N.; Yu, K.; Wu, M.; Haller, E. E.; *et al.* Black Ge Based on Crystalline/Amorphous Core/Shell Nanoneedle Arrays. *Nano Lett.* **2010**, *10*, 520–523.
- Liu, C. H.; Chen, C. H.; Chen, S. Y.; Yen, Y. T.; Kuo, W. C.; Juang, J. Y.; Liao, Y. K.; Kuo, H. C.; Lai, C. H.; Chen, L. J. Large Scale Single-Crystal Cu (in, Ga) Se₂ Nanotip Arrays for High Efficiency Solar Cell. *Nano Lett.* **2011**, *11*, 4443–4448.
- Garnett, E. C.; Yang, P. D. Light Trapping in Silicon Nanowire Solar Cells. *Nano Lett.* **2010**, *10*, 1082–1087.
- Kelzenberg, M. D.; Boettcher, S. W.; Petykiewicz, J. A.; Turner-Evans, D. B.; Putnam, M. C.; Warren, E. L.; Spurgeon, J. M.; Briggs, R. M.; Lewis, N. S.; Atwater, H. A. Enhanced Absorption and Carrier Collection in Si Wire Array for Photovoltaic Applications. *Nat. Mater.* **2010**, *9*, 239–244.
- Chang, H.; Lai, K.; Dai, Y.; Wang, H.; Lin, C.; He, J. Nanowire Arrays with Controlled Structure Profiles for Maximizing Optical Collection Efficiency. *Energy Environ. Sci.* **2011**, *4*, 2863–2869.
- Shin, J. C.; Kim, K. H.; Yu, K. J.; Hu, H.; Yin, L.; Ning, C.; Rogers, J. A.; Zuo, J.; Li, X. In_(x)Ga_(1-x) as Nanowires on Silicon: One-Dimensional Heterogeneous Epitaxy, Bandgap Engineering, and Photovoltaics. *Nano Lett.* **2011**, *11*, 4831–4838.
- Fan, Z. Y.; Kapadia, R.; Leu, P. W.; Zhang, X. B.; Chueh, Y. L.; Takei, K.; Yu, K.; Jamshidi, A.; Rathore, A. A.; Ruebusch, D. J.; *et al.* Ordered Arrays of Dual-Diameter Nanopillars for Maximized Optical Absorption. *Nano Lett.* **2010**, *10*, 3823–3827.
- Fan, Z. Y.; Razavi, H.; Do, J. W.; Moriwaki, A.; Ergen, O.; Chueh, Y. L.; Leu, P. W.; Ho, J. C.; Takahashi, T.; Reichertz, L. A.; *et al.* Three Dimensional Nanopillar Array Photovoltaics on Low Cost and Flexible Substrate. *Nat. Mater.* **2009**, *8*, 648–653.
- Han, S. E.; Chen, G. Optical Absorption Enhancement in Silicon Nanohole Arrays for Solar Photovoltaics. *Nano Lett.* **2010**, *10*, 1012–1015.
- Peng, K.; Wang, X.; Li, L.; Wu, X.; Lee, S. High-Performance Silicon Nanohole Solar Cells. *J. Am. Chem. Soc.* **2010**, *132*, 6872–6873.
- Wang, B.; Leu, P. W. Enhanced Absorption in Silicon Nanocone Arrays for Photovoltaics. *Nanotechnology* **2012**, *23*, 194003.
- Chen, H.; Chuang, S.; Lin, C.; Lin, Y. Using Colloidal Lithography to Fabricate and Optimize Sub-Wavelength Pyramidal and Honeycomb Structures in Solar Cells. *Opt. Express* **2007**, *15*, 14793–14803.
- Han, S. E.; Chen, G. Toward the Lambertian Limit of Light Trapping in Thin Nanostructured Silicon Solar Cells. *Nano Lett.* **2010**, *10*, 4692–4696.
- Mavrokefalos, A.; Han, S. E.; Yerci, S.; Branham, M. S.; Chen, G. Efficient Light Trapping in Inverted Nanopyramid Thin Crystalline Silicon Membranes for Solar Cell Applications. *Nano Lett.* **2012**, *12*, 2792–2796.
- Yao, Y.; Yao, J.; Narasimhan, V. K.; Ruan, Z.; Xie, C.; Fan, S. H.; Cui, Y. Broadband Light Management Using Low-Q Whispering Gallery Modes in Spherical Nanoshells. *Nat. Commun.* **2012**, *3*, 664–670.
- Grandidier, J.; Weitekamp, R. A.; Deceglie, M. G.; Callahan, D. M.; Battaglia, C.; Bukowsky, C. R.; Ballif, C.; Grubbs, R. H.; Atwater, H. A. Solar Cell Efficiency Enhancement via Light Trapping in Printable Resonant Dielectric Nanosphere Arrays. *Phys. Status Solidi A* **2012**, *10.1002/pssa.201228690*.
- Grandidier, J.; Callahan, D. M.; Munday, J. N.; Atwater, H. A. Light Absorption Enhancement in Thin-Film Solar Cells Using Whispering Gallery Modes in Dielectric Nanospheres. *Adv. Mater.* **2011**, *23*, 1272–1276.
- Jessensky, O.; Muller, F.; Gosele, U. Self-Organized Formation of Hexagonal Pore Arrays in Anodic Alumina. *Appl. Phys. Lett.* **1998**, *72*, 1173–1175.
- Steinhart, M.; Wendorff, J. H.; Greiner, A.; Wehrspohn, R. B.; Nielsch, K.; Schilling, J.; Choi, J.; Gosele, U. Polymer Nanotubes by Wetting of Ordered Porous Templates. *Science* **2002**, *296*, 1997.
- Fan, Z. Y.; Dutta, D.; Chien, C. J.; Chen, H. Y.; Brown, E. C.; Chang, P. C.; Lu, J. G. Electrical and Photoconductive Properties of Vertical ZnO Nanowires in High Density Arrays. *Appl. Phys. Lett.* **2006**, *89*, 213110–213112.
- Ergen, O.; Ruebusch, D. J.; Fang, H.; Rathore, A. A.; Kapadia, R.; Fan, Z.; Takei, K.; Jamshidi, A.; Wu, M.; Javey, A. Shape-Controlled Synthesis of Single-Crystalline Nanopillar Arrays by Template-Assisted Vapor–Liquid–Solid Process. *J. Am. Chem. Soc.* **2010**, *132*, 13972–13974.
- Masuda, H.; Yada, K.; Osaka, A. Self-Ordering of Cell Configuration of Anodic Porous Alumina with Large-Size Pores in Phosphoric Acid Solution. *Jpn. J. Appl. Phys.* **1998**, *37*, L1340–L1342.

27. Choi, J.; Luo, Y.; Wehrspohn, R. B.; Hillebrand, R.; Schilling, J.; Gosele, U. Perfect Two-Dimensional Porous Alumina Photonic Crystals with Duplex Oxide Layers. *J. Appl. Phys.* **2003**, *94*, 4757–4762.
28. Garnett, E. C.; Brongersma, M. L.; Cui, Y.; McGehee, M. D. Nanowire Solar Cells. *Annu. Rev. Mater. Res.* **2011**, *41*, 269–295.
29. Yeh, L. K.; Lai, K. Y.; Lin, G. J.; Fu, P. H.; Chang, H. C.; Lin, C. A.; He, J. H. Giant Efficiency Enhancement of GaAs Solar Cells with Graded Antireflection Layers Based on Syringelike ZnO Nanorod Arrays. *Adv. Energy Mater.* **2011**, *1*, 506–510.
30. Hsu, C. M.; Battaglia, C.; Pahud, C.; Ruan, Z.; Haug, F. J.; Fan, S.; Ballif, C.; Cui, Y. High-Efficiency Amorphous Silicon Solar Cell on a Periodic Nanocone Back Reflector. *Adv. Eng. Mater.* **2012**, *2*, 628–633.
31. Battaglia, C.; Hsu, C. M.; Soderstrom, K.; Escarré, J.; Haug, F. J.; Charrière, M.; Boccard, M.; Despeisse, M.; Alexander, D. T. L.; Cantoni, M. Light Trapping in Solar Cells: Can Periodic Beat Random?. *ACS Nano* **2012**, *6*, 2790–2797.
32. Zhu, J.; Hsu, C.; Yu, Z.; Fan, S.; Cui, Y. Nanodome Solar Cells with Efficient Light Management and Self-Cleaning. *Nano Lett.* **2010**, *10*, 1979–1984.
33. Battaglia, C.; Escarre, J.; Soederstroem, K.; Erni, L.; Ding, L.; Bugnon, G.; Billet, A.; Boccard, M.; Barraud, L.; De Wolf, S.; *et al.* Nanoimprint Lithography for High-Efficiency Thin-Film Silicon Solar Cells. *Nano Lett.* **2011**, *11*, 661–665.
34. Staebler, D.; Wronski, C. Reversible Conductivity Changes in Discharge-Produced Amorphous Si. *Appl. Phys. Lett.* **1977**, *31*, 292–294.
35. *Air Mass 1.5 Spectra*; American Society for Testing and Materials: West Conshohocken, PA; 2003 <http://rredc.nrel.gov/solar/spectra/am1.5/>.
36. Hutley, M. C. In *Diffraction Gratings (Techniques of Physics)*; March, N. H., Daghlish, H. N., Eds.; Academic Press: London, 1982.